MOLECULAR IMAGING AND BIOLOGY

Mol Imaging Biol (2020) 22:444–452
DOI: 10.1007/s11307-019-01387-6

Published Online: 17 June 2019

RESEARCH ARTICLE

Validation of Parametric Methods for [^{11}C]UCB-J PET Imaging Using Subcortical White Matter as Reference Tissue

Nathalie Mertens,[1,2] Ralph Paul Maguire,[3] Kim Serdons,[1] Brigitte Lacroix,[3] Joel Mercier,[3] David Sciberras,[3] Koen Van Laere,[1] Michel Koole[1]

[1]*Department of Nuclear Medicine and Molecular Imaging, KU Leuven, Leuven, Belgium*
[2]*Division of Nuclear Medicine, KU Leuven, Herestraat 49, 3000, Leuven, Belgium*
[3]*UCB Pharma, Braine-l'Alleud, Belgium*

Abstract

Purpose: The aim of this study was to evaluate different non-invasive methods for generating (R)-1-((3-([^{11}C]methyl)pyridin-4-yl)methyl)-4-(3,4,5-trifluorophenyl)pyrrolidin-2-one) ([^{11}C]UCB-J) parametric maps using white matter (centrum semi-ovale–SO) as reference tissue.

Procedures: Ten healthy volunteers (8 M/2F; age 27.6 ± 10.0 years) underwent a 90-min dynamic [^{11}C]UCB-J positron emission tomography (PET) scan with full arterial blood sampling and metabolite analysis before and after administration of a novel chemical entity with high affinity for presynaptic synaptic vesicle glycoprotein 2A (SV2A). A simplified reference tissue model (SRTM2), multilinear reference tissue model (MRTM2), and reference Logan graphical analysis (rLGA) were used to generate binding potential maps using SO as reference tissue (BP_{SO}). Shorter dynamic acquisitions down to 50 min were also considered. In addition, standard uptake value ratios (SUVR) relative to SO were evaluated for three post-injection intervals ($SUVR_{SO,40\text{-}70min}$, $SUVR_{SO,50\text{-}80min}$, and $SUVR_{SO,60\text{-}90min}$ respectively). Regional parametric BP_{SO} + 1 and $SUVR_{SO}$ were compared with regional distribution volume ratios of a 1-tissue compartment model (1TCM DVR_{SO}) using Spearman correlation and Bland-Altman analysis.

Results: For all methods, highly significant correlations were found between regional, parametric BP_{SO} + 1 (r = [0.63;0.96]) or $SUVR_{SO}$ (r = [0.90;0.91]) estimates and regional 1TCM DVR_{SO}. For a 90-min dynamic scan, parametric SRTM2 and MRTM2 values presented similar small bias and variability (– 3.0 ± 2.9 % for baseline SRTM2) and outperformed rLGA (– 10.0 ± 5.3 % for baseline rLGA). Reducing the dynamic acquisition to 60 min had limited impact on the bias and variability of parametric SRTM2 BP_{SO} estimates (– 1.0 ± 9.9 % for baseline SRTM2) while a higher variability (– 1.83 ± 10.8 %) for baseline MRTM2 was observed for shorter acquisition times. Both $SUVR_{SO,60\text{-}90min}$ and $SUVR_{SO,50\text{-}80min}$ showed similar small bias and variability (– 2.8 ± 4.6 % bias for baseline $SUVR_{SO,60\text{-}90min}$).

Conclusion: SRTM2 is the preferred method for a voxelwise analysis of dynamic [^{11}C]UCB-J PET using SO as reference tissue, while reducing the dynamic acquisition to 60 min has limited

Electronic supplementary material The online version of this article (https://doi.org/10.1007/s11307-019-01387-6) contains supplementary material, which is available to authorized users.

Correspondence to: Nathalie Mertens; *e-mail:* nathalie.mertens@kuleuven.be

impact on [^{11}C]UCB-J BP_{SO} parametric maps. For a static PET protocol, both $SUVR_{SO,60-90min}$ and $SUVR_{SO,50-80min}$ images are an excellent proxy for [^{11}C]UCB-J BP_{SO} parametric maps.

Key words: Synaptic density, [^{11}C]UCB-J PET, Parametric maps, Reference tissue, Subcortical white matter

Introduction

Synaptic pathology is associated with many neurological and psychiatric disorders. For example, in patients with epilepsy, reduced synaptic density has been reported in the seizure onset zone [1–3],while a close relation between cognitive impairment and decreased synaptic density has been reported in the hippocampus and cerebral cortex of patients with Alzheimer's disease [4, 5]. Moreover, in stroke, traumatic brain injury, and psychiatric disorders, such as autism [6], depression [7], and schizophrenia [8, 9], synaptic density changes have been associated with clinical deficiencies and are thought to play a role in the phenotyping of these diseases.

(R)-1-((3-([^{11}C]methyl)pyridin-4-yl)methyl)-4-(3,4,5-trifluorophenyl)pyrrolidin-2-one) ([^{11}C]UCB-J) has been developed as positron emission tomography (PET) ligand with high affinity and specificity for synaptic vesicle glycoprotein 2A (SV2A) [10–12]. SV2A is an integral membrane protein, located in the presynaptic vesicle membrane and expressed ubiquitously in all synapses across the brain and so [^{11}C]UCB-J has been used to enable *in vivo* imaging of synaptic density. [^{11}C]UCB-J uptake has very good pharmacokinetics and quantification properties enabling a 1-tissue compartment model (1TCM) as the most appropriate model to describe tracer kinetics in brain tissue [11]. Furthermore, subcortical white matter, and more specifically the centrum semi-ovale (SO), has been validated as a suitable reference tissue for non-invasive quantification of synaptic density in the human brain using [^{11}C]UCB-J PET imaging [13]. To further facilitate a voxelwise analysis of [^{11}C]UCB-J PET data, we evaluated different approaches to generate [^{11}C]UCB-J parametric maps using SO as reference tissue. For this purpose, we compared regional values of different reference tissue parametric methods with regional 1TCM distribution volume ratios relative to SO (DVR_{SO}). As a shorter acquisition time may facilitate research on synaptic pathology and further improve clinical applicability, we evaluated the time stability of the parametric maps by reducing the acquisition time down to 50-min post injection. We also considered standard uptake value ratios relative to SO ($SUVR_{SO}$) as a simplified reference tissue approach and evaluated several 30-min static acquisition time intervals for determining $SUVR_{SO}$.

Materials and Methods

[^{11}C]UCB-J PET/MR Imaging

Dynamic PET data were acquired in a PET dose occupancy study to evaluate receptor occupancy of padsevonil (UCB Pharma, Brussels, Belgium), a novel chemical entity with high affinity for presynaptic SV2A [13]. Data for this dynamic PET study were previously published by Koole et al. [13]. In total, ten healthy volunteers (8 males and 2 females, age 27.6 ± 10.0 years (mean ± SD) with an age range of 20 to 54 years) participated in this study. Subjects were carefully screened for medical history and underwent a physical and neurological examination, vital signs recording, an electrocardiogram, urine analysis, laboratory blood tests, drug and alcohol screen, and pregnancy tests for females. The study was conducted at the University Hospital Leuven, Belgium and approved by the local Ethics Committee (University Hospitals Leuven/KU Leuven) and each subject signed a written informed consent before enrollment. All volunteers underwent 90-min dynamic [^{11}C]UCB-J PET/magnetic resonance (MR) scanning with arterial blood sampling before and after the oral administration of a single dose of padsevonil (6.25–100 mg). This resulted in 10 [^{11}C]UCB-J PET scans under baseline conditions and 17 [^{11}C]UCB-J PET scans under blocking conditions as 7 subjects received two [^{11}C]UCB-J PET scans at two different time points after drug administration. The 17 post dose PET scan were performed at 2 h (7 scans), 6 h (4 scans), 24 h (3 scans), 27 h (1 scan), and 30 h (2 scans) after drug administration. Details of the image acquisition and reconstruction parameters on the GE Signa PET/MR are given in the Electronic Supplementary Materials. The synthesis, radiolabeling, and quality control of [^{11}C]UCB-J were done according to the same procedure as described by Koole et al. [13]. The injected activity of [^{11}C]UCB-J was 232.6 ± 67.7 MBq (mean ± SD), with a specific activity of 91.3 ± 38.2 GBq/μmol and injected UCB-J mass dose of 0.98 ± 0.63 μg.

Regional time activity curves (TACs) were extracted in PMOD (version 3.905) by projecting a simplified Hammers atlas [14] on the dynamic PET data. PET data were spatially normalized to Montreal Neurological Institute (MNI) space using SPM8 (Statistical Parametric Mapping, MATLAB 2018b, the MathWorks, Inc.), and simultaneously acquired 3D T1-weighted MR data. Volume of interests (VOIs) were restricted to gray matter by applying a simple threshold of 0.3 to the individual gray matter probability maps resulting from an SPM-based multichannel MR segmentation. Volumes of interest (VOIs) for the frontal, temporal, parietal, and occipital cortex as well as the insula, anterior and posterior cingulate, striatum, thalamus, hippocampus, amygdala, and cerebellum were determined. From all cortical VOIs, a composite cortical VOI was created to extract overall cortical TACs from the dynamic PET data.

Additionally, the centrum semi-ovale was delineated by performing isotropic Gaussian smoothing (7-mm FWHM) to the individual white matter probability maps and applying a 0.99 threshold to the appropriate slices to include only voxels with a high probability of being part of the centrum semi-ovale. Since a 1-tissue compartment model (1TCM) was identified as the most appropriate model to describe [^{11}C]UCB-J tracer kinetics in brain tissue, regional distribution volume estimates (V_T) were determined by applying 1TCM to the 90-min regional TAC data with a fixed blood volume of 5 %. A composite cortical TAC was used to estimate the potential small time shift between the PET TAC and arterial blood/plasma input functions. Baseline cortical V_T was 5.54 ± 0.47 (mean ± SD, range [4.85, 6.56]) and post drug cortical V_T was 2.55 ± 1.39 ([0.76, 5.43]), yielding an overall cortical V_T of 3.66 ± 1.85 (range [0.76, 6.56]). Lassen plots taking into account baseline and post drug regional V_T values were used to determine SV2A occupancy [15], which varied across the range of 2.2 % to 99.3 % (mean ± SD 65.0 ± 29.7 %).

As the centrum semi-ovale (SO) was established as an acceptable region for non-displaceable [^{11}C]UCB-J uptake in brain tissue, regional distribution volume ratios relative to SO, determined as V_T/V_{SO} and denoted as $DVR_{SO,90}$, were considered as reference values for method comparison based on a 90-min acquisition.

[^{11}C]UCB-J PET Parametric Mapping

For parametric approaches using a reference tissue, a simplified reference tissue model using a set of predefined basis functions (SRTM2) [16], a multilinear reference tissue model (MRTM2) [17], and a reference Logan graphical analysis (rLGA) [18] were considered. For all three approaches, the tracer efflux rate constant k_2 from the reference tissue to plasma was assumed to be known and set to a fixed value. This washout constant was determined prior to the parametric mapping by a regional SRTM approach with k_2 coupled between all brain regions to obtain a global, robust estimate. SRTM2 and MRTM2 resulted in parametric binding potential maps using SO as reference tissue (BP_{SO}); while for rLGA, parametric maps of the binding potential were estimated as voxelwise distribution volume ratios minus 1 (DVR-1). Next to binding potential mapping (BP_{SO}), relative tracer delivery maps (R_1) were determined by the SRTM2 and MRTM2 approaches. For both the parametric binding potential and relative tracer delivery maps, regional parametric estimates were calculated by projecting VOIs (as defined above) on these parametric maps and compared with regional 1CTM DVR-1 values and with the ratio of regional 1TCM influx rate constants K_1 relative to SO respectively.

The impact of a reduction in acquisition time on the regional parametric BP_{SO} and R_1 estimates was evaluated by considering acquisition times of 90 min, 80 min, 70 min, 60 min, and 50 min, starting at the time of tracer injection ($BP_{SO,90}$, $BP_{SO,80}$, $BP_{SO,70}$, $BP_{SO,60}$, and $BP_{SO,50}$ respectively and $R_{1,90}$, $R_{1,80}$, $R_{1,70}$, $R_{1,60}$, and $R_{1,50}$ respectively).

Finally, a standard uptake value ratio relative to SO ($SUVR_{SO}$) of a single static PET frame post injection was evaluated as a parametric approach for voxelwise SUVR-1 estimates. For the static PET frame, a 30-min acquisition interval from 40- to 70-, 50- to 80-, and 60- to 90-min post injection was considered ($SUVR_{SO,40–70}$, $SUVR_{SO,50–80}$, and $SUVR_{SO,60–90}$ respectively).

Statistics

Spearman correlation and linear regression analysis (line forced through the origin) were performed for all conditions and for baseline and post drug conditions separately, to evaluate the relationship between regional 1TCM DVR_{SO} values and regional parametric $BP_{SO} + 1$ or $SUVR_{SO}$ estimates obtained by the different parametric reference tissue models for different acquisition time intervals. The same statistical analysis was performed to evaluate the relationship between regional 1TCM $K_1/K_{1,SO}$ ratios and regional parametric R_1 values estimated by SRTM2 and MRTM2 for different acquisition times, again for all conditions and for baseline and post drug conditions separately.

Next, a Bland-Altman analysis was used to evaluate the agreement between regional 1TCM DVR_{SO} and regional parametric $BP_{SO} + 1$ or $SUVR_{SO}$ estimates obtained by the different parametric reference tissue models for different acquisition time intervals. For all conditions, the difference between regional 1TCM DVR_{SO} and parametric $BP_{SO} + 1$ or $SUVR_{SO}$ was considered for the analysis while for baseline conditions, the relative difference was used. A Bland-Altman analysis was also performed to evaluate the correspondence between 1TCM $K_1/K_{1,SO}$ ratios and regional parametric R_1 values estimated by SRTM2 and MRTM2 for different acquisition times by considering relative differences for pooled baseline and post drug scans.

Results

The washout constant, k_2, estimated in all brain regions, was compared between the acquisition times. Average values remained the same for all acquisition times, while the variance increases for shorter acquisitions (see Fig. 1). MRTM2 and SRTM2 failed for 1 out of the 27 scans (4 %), 2 out of 27 scans (7 %), and 3 out of 27 scans (11 %) for a 70-, 60-, and 50-min acquisitions respectively. For these cases, the problematic estimation of the reference washout rate constant could be explained by the high R_1 values. These high R_1 values are required for SRTM2 to accommodate the difference in tracer uptake between the gray matter and reference white matter. However, the washout rate constant of white matter is related to the

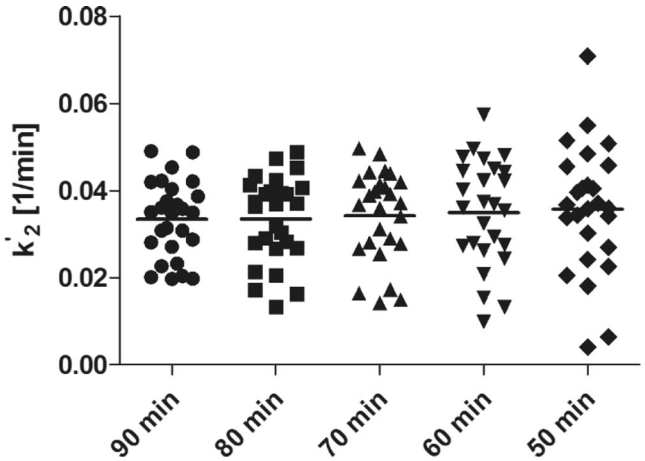

Fig. 1 Scatter plots of efflux rate constant between reference tissue and plasma (k'_2) calculated by a VOI based SRTM2 approach, resulting in a coupled efflux rate constant for all brain regions. Efflux rate constants are calculated for acquisition times of 90, 80, 70, 60, and 50 min.

washout rate constant of the target tissue by a factor which is inversely proportional to R_1. Therefore, underestimation of the target washout rate constant by using a shorter acquisition time could result in low reference washout rate constants.

For the full 90-min acquisition, highly significant and strong correlations (all $p < 0.0001$) were found between regional 1TCM DVR_{SO} values and regional parametric SRTM2, MRTM2, and rLGA $BP_{SO,90} + 1$ estimates, with a slightly lower correlation value for rLGA $BP_{SO,90} + 1$ values (see Table 1). The linear regression slope was close to 1.00 for regional parametric SRTM2 and MRTM2 estimates. For regional parametric rLGA, a slightly higher bias was observed. For the static $SUVR_{SO}$ approach, highly significant correlations ($p < 0.0001$) were observed between regional 1TCM DVR_{SO} and $SUVR_{SO}$ values for 60- to 90-, 50- to 80-, and 40- to 70-min post-injection, with an increasing bias for early 40- to 70-min post-injection time interval. Overall, Spearman rho, slope, and goodness of fit of the linear regression were consistently lower for baseline scanning compared to post drug scanning. This was confirmed by visual assessment of the scatter plots of cortical parametric SRTM2 $BP_{SO,90} + 1$ *versus* regional 1TCM DVR_{SO} values as presented in Fig. 2, demonstrating a less optimal straight line fit for baseline conditions. Representative parametric images of baseline SRTM2, MRTM2, and rLGA $BP_{SO,90} + 1$ and $SUVR_{SO}$ from a healthy subject are given in Fig. 3.

A Bland-Altman analysis comparing regional parametric SRTM2 and MRTM2 $BP_{SO,90} + 1$ with regional 1TCM DVR_{SO} (difference *vs* mean) revealed a small, negative bias with a similar 95 % limits of agreement interval when taking into account all conditions while rLGA $BP_{SO,90} + 1$ demonstrated a substantial higher bias with a two-fold larger 95 % limits of agreement interval (see Table 2). This was confirmed by the Bland-Altman analysis (%difference *vs* mean) of baseline conditions where regional parametric SRTM2 and MRTM2 $BP_{SO,90} + 1$ estimates clearly outperformed regional parametric rLGA $BP_{SO,90} + 1$ values since the latter demonstrated a -10.0 ± 5.4 % bias compared to the respective biases of -3.0 ± 2.9 % and -2.8 ± 2.8 % of the former two. For this reason, we restricted the analysis of time stability of BP_{SO} for shorter

Table 1. Spearman correlation and linear regression analysis (straight line through the origin) between regional 1TCM DVR_{SO} values and regional parametric SRTM2 $BP_{SO} + 1$, MRTM2 $BP_{SO} + 1$, and rLGA $BP_{SO,90} + 1$ estimates for different acquisition time intervals (90, 80, 70, 60, and 50 min) and between regional 1TCM DVR_{SO} values and regional $SUVR_{SO,40–70}$, $SUVR_{SO,50–80}$, and $SUVR_{SO,60–90}$ values for a 40- to 70-, 50- to 80-, and 60- to 90-min post-injection acquisition time interval. All approaches used the centrum semi-ovale (SO) as reference tissue. Data of baseline and post drug scans were reported both separately and pooled together. All correlations were highly significant ($p < 0.0001$)

	Baseline ($N = 10$)			Post drug ($N = 17$))			Baseline and post drug ($N = 27$)		
	Spearman rho	Slope	Goodness of fit (Sy,x)	Spearman rho	Slope	Goodness of Fit (Sy,x)	Spearman rho	Slope	Goodness of fit (Sy,x)
SRTM2 $BP_{SO} + 1$									
90 min	0.96	0.97	0.15	1.00	0.99	0.14	1.00	0.98	0.15
80 min	0.93	0.99	0.24	1.00	1.00	0.12	0.99	0.99	0.18
70 min	0.84	1.01	0.49	1.00	0.98	0.15	0.98	1.00	0.33
60 min	0.77	0.99	0.59	1.00	0.98	0.18	0.98	0.99	0.39
50 min	0.63	0.93	0.62	0.95	0.94	0.32	0.96	0.94	0.46
MRTM2 $BP_{SO} + 1$									
90 min	0.96	0.97	0.15	1.00	0.99	0.14	1.00	0.98	0.15
80 min	0.94	0.99	0.27	1.00	1.00	0.11	0.99	1.00	0.19
70 min	0.83	1.03	0.61	1.00	0.99	0.15	0.98	1.04	1.34
60 min	0.79	0.99	0.70	1.00	0.98	0.18	0.98	0.98	0.44
50 min	0.65	0.95	0.67	0.99	0.97	0.18	0.97	0.96	0.43
rLGA $BP_{SO} + 1$									
90 min	0.89	0.90	0.27	0.99	0.94	0.16	0.99	0.91	0.22
$SUVR_{SO}$									
60–90 min	0.91	0.97	0.25	0.99	0.95	0.16	0.99	0.97	0.20
50–80 min	0.90	0.96	0.25	1.00	0.96	0.15	0.99	0.96	0.19
40–70 min	0.90	0.92	0.30	1.00	0.95	0.16	0.99	0.93	0.23

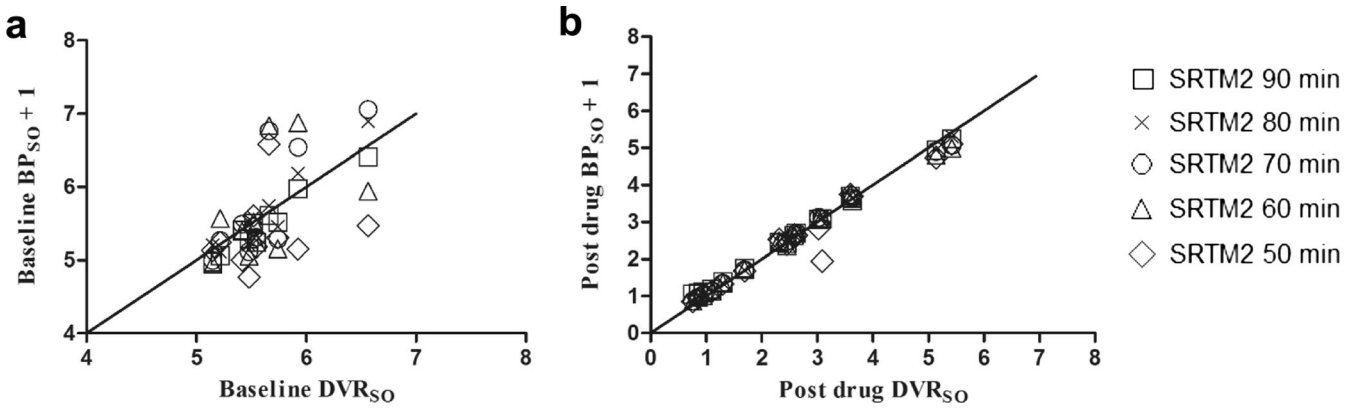

Fig. 2 Scatter plots for cortical parametric SRTM2 $BP_{SO} + 1$ estimates using an acquisition time of 90, 80, 70, 60, and 50 min *vs* 1TCM DVR_{SO} values for both **a** baseline and **b** post drug conditions.

acquisition time intervals to regional parametric SRTM2 and MRTM2 BP_{SO} estimates. A Bland-Altman analysis comparing regional $SUVR_{SO,40–70}$, $SUVR_{SO,50–80}$, and $SUVR_{SO,60–90}$ values with regional 1TCM DVR_{SO} revealed a small, negative bias with a similar 95 % limits of agreement interval for regional $SUVR_{SO,50–80}$ and $SUVR_{SO,60–90}$ values when taking into account all conditions and baseline conditions separately (see Table 2). On the other hand, $SUVR_{SO,40–70}$ demonstrated a higher bias with an increased 95 % limits of agreement interval with a negative bias of -7.8 ± 6.0 % compared to the -4.0 ± 4.7 % and -2.8 ± 4.6 % bias of regional $SUVR_{SO,50–80}$ and $SUVR_{SO,60–90}$ respectively.

In terms of time stability, Spearman rho and slope of the linear regression are very similar for both regional parametric SRTM2 and MRTM2 $BP_{SO} + 1$ values for a shorter acquisition time compared to the 1TCM DVR_{SO} values using the 90-min dynamic PET data (see Table 1). On the other hand, goodness of fit values for regional parametric SRTM2 $BP_{SO} + 1$ values, representing the root mean square error, slightly increase for shorter acquisition times, indicating a less optimal straight line fit for these reference tissue approaches (see Table 1). The same trend has been observed for both SRTM2 and MRTM2 $BP_{SO} + 1$ values with slightly higher goodness of fit values for the latter. These findings were consistent for both baseline and post drug conditions

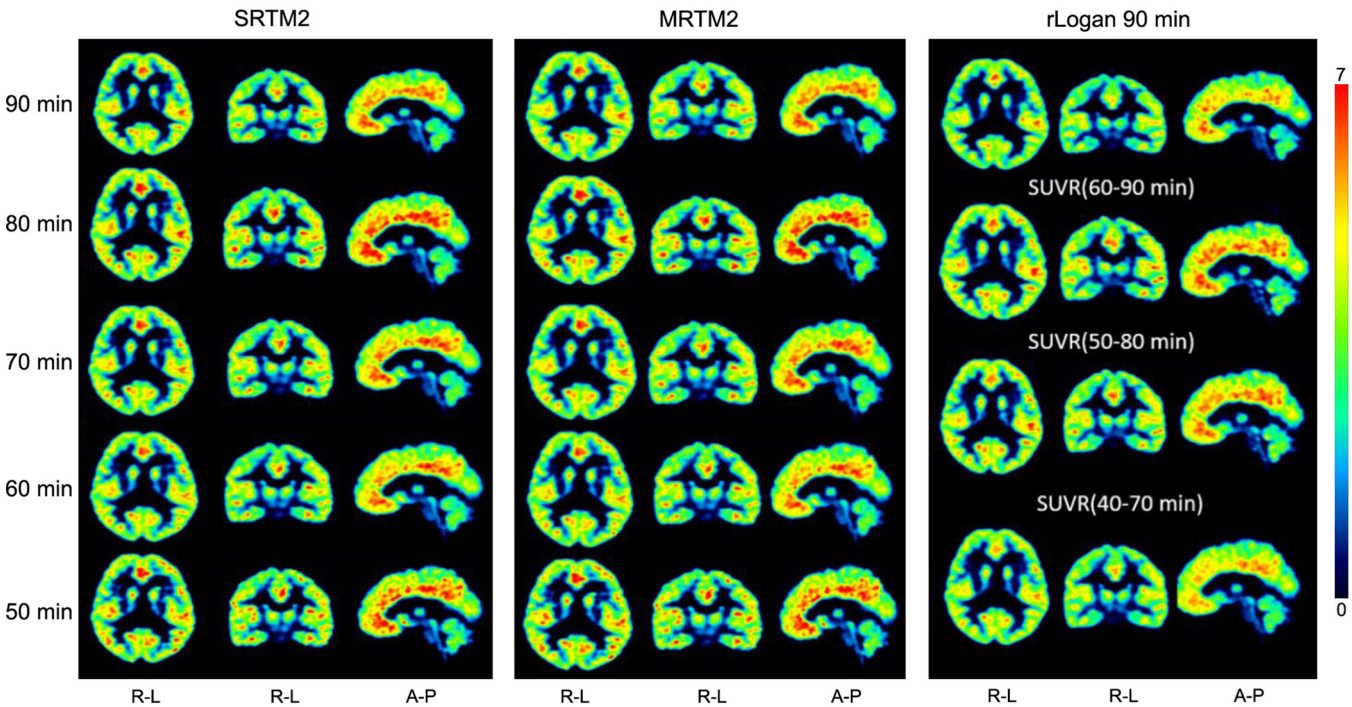

Fig. 3 Parametric $BP_{SO} + 1$ maps of a baseline scan of a healthy volunteer (M, 23 years, 93 kg, 197 MBq [11C]UCB-J) using centrum semi-ovale (SO) as reference tissue. Images are in radiological orientation.

and were in line with the visual assessment of the scatter plots of cortical parametric SRTM2 $BP_{SO}+1$ *versus* regional 1TCM DVR_{SO} for different acquisition time intervals (see Fig. 2), demonstrating a less optimal straight line fit for shorter acquisition times. A Bland-Altman analysis comparing regional parametric SRTM2 and MRTM2 $BP_{SO}+1$ for shorter acquisition times with regional 1TCM DVR_{SO} confirmed that reducing the acquisition time down to 60 min did not have a significant impact on parametric SRTM2 and MRTM2 $BP_{SO}+1$ estimates, while a higher variability has been observed for the latter (see Table 2).

In terms of parametric R_1 maps, highly significant correlations ($p<0.0001$) were observed between regional 1TCM K_1 ratios relative to SO and regional parametric SRTM2 and MRTM2 R_1 estimates for an acquisition times down to 50 min. Linear regression analysis, slope values, indicative for bias, and goodness of fit values were similar for both approaches, independent of scanning time (Table 3). A Bland-Altman analysis comparing regional 1TCM K_1 ratios relative to SO values with regional, parametric SRTM2, and MRTM2 R_1 estimates revealed a small negative bias and similar 95 % limits of agreement interval for both approaches which remained constant as the acquisition time was shortened. Representative parametric R_1 maps of a healthy subject under baseline conditions are given in Fig. 4.

Discussion

As accurate and quantitative parametric maps are a prerequisite for clinical applications and voxelwise analysis, the purpose of this study was to evaluate different non-invasive parametric methods for [^{11}C]UCB-J PET imaging of the human brain. Since subcortical white matter was already identified as a suitable reference tissue for [^{11}C]UCB-J brain PET quantification [13], we evaluated both reference tissue methods using SO as reference tissue and SUVR relative to SO as parametric approaches. As reference values, we used regional 1TCM DVR_{SO} relative to SO since previous studies demonstrated that 1TCM is the most appropriate model for [^{11}C]UCB-J tracer kinetics in brain tissue.

In terms of reference tissue methods, we considered MRTM2 and rLGA, next to SRTM2, and assumed foreknowledge about the efflux rate constant between reference tissue and plasma for generating the parametric maps. For all three approaches, the tracer efflux rate constant k_2 from the reference tissue to plasma was set to a fixed value. As such, the number of parameters was limited to two, therefore reducing the impact of noise on the parameter estimation [19]. In order to *a priori* estimate the efflux rate constant between reference tissue and plasma, we used a VOI-based SRTM2 approach and coupled the efflux rate constant from the reference tissue back to the plasma for all brain regions to give a global, more robust estimate. For this *a priori* estimation, SRTM2 was used since this reference tissue model assumes 1TCM to be a suitable model for tracer kinetics in both the reference and target brain tissue and this was confirmed for [^{11}C]UCB-J kinetics in brain tissue. Regarding time stability, we evaluated parametric $BP_{SO}+1$ maps using SO as reference region for a 50-, 60-, 70-, 80-, and 90-min dynamic PET data starting at tracer injection. Findings demonstrated that a dynamic PET scan of at least 60 min is required to achieve accurate quantification using a

Table 2. Bland-Altman analysis comparing regional 1TCM DVR_{SO} with regional parametric SRTM2, MRTM2, and rLGA $BP_{SO}+1$ estimates and with regional $SUVR_{SO}$ for baseline conditions (%difference *vs* mean) and pooled baseline and post drug scans (difference *vs* mean). For regional parametric SRTM2 and MRTM2 $BP_{SO}+1$ estimates, an acquisition time of 90, 80, 70, 60, and 50 min was considered starting at the time of tracer injection while for $SUVR_{SO}$ a 40- to 70-, 50- to 80-, and 60- to 90-min acquisition after tracer injection was evaluated. All approaches used the centrum semi-ovale (SO) as reference brain tissue

	Baseline ($N=10$) (%difference *vs* mean)			Baseline and post drug ($N=27$) (difference *vs* mean)		
	Difference (%)	SD (%)	95 % limits of agreement (%)	Difference	SD	95 % limits of agreement
SRTM2 $BP_{SO}+1$						
90 min	−2.98	2.86	[−8.59, 2.63]	−0.039	0.17	[−0.38, 0.30]
80 min	−1.26	4.25	[−9.59, 7.07]	−0.0028	0.18	[−0.35, 0.35]
70 min	0.42	8.45	[−16.14, 16.98]	0.026	0.33	[−0.62, 0.68]
60 min	−1.00	9.89	[−20.39, 18.38]	−0.016	0.40	[−0.79, 0.76]
50 min	−6.45	11.44	[−28.87, 15.98]	−0.19	0.49	[−1.15, 0.77]
MRTM2 $BP_{SO}+1$						
90 min	−2.84	2.80	[−8.33, 2.66]	−0.037	0.17	[−0.36, 0.29]
80 min	−0.92	4.55	[−9.84, 8.00]	0.0044	0.19	[−0.36, 0.37]
70 min	2.46	14.89	[−26.72, 31.63]	0.12	1.34	[−2.50, 2.75]
60 min	−1.83	10.83	[−23.04, 19.39]	−0.029	0.45	[−0.91, 0.85]
50 min	−4.71	11.73	[−27.70, 18.28]	−0.11	0.45	[−0.99, 0.78]
rLGA $BP_{SO}+1$						
90 min	−10.01	5.35	[−20.50, 0.48]	−0.26	0.33	[−0.90, 0.39]
$SUVR_{SO}$						
60–90 min	−2.82	4.57	[−11.78, 6.14]	−0.17	0.18	[−0.52, 0.18]
50–80 min	−3.95	4.70	[−13.16, 5.25]	−0.17	0.19	[−0.65, 0.19]
40–70 min	−7.83	5.97	[−19.52, 3.87]	−0.26	0.27	[−0.79, 0.26]

Table 3. Spearman correlation, linear regression analysis (line through the origin), and Bland-Altman analysis (%difference *vs* mean) between regional 1TCM $K_1/K_{1,SO}$ values and SRTM2 R_1 and MRTM2 R_1 values for different acquisition time intervals (90, 80, 70, 60, and 50 min). The centrum semi-ovale (SO) was used as reference tissue. Baseline and post drug scans were pooled together ($N = 27$). All correlations were highly significant ($p < 0.0001$)

	Spearman correlation and linear regression analysis			Bland-Altman analysis (%difference *vs* mean)		
	Spearman rho	Slope	Goodness of fit (Sy,x)	Difference (%)	SD (%)	95 % limits of agreement (%)
SRTM2 R_1						
90 min	0.94	0.99	0.22	− 0.28	6.00	[− 12.03, 11.48]
80 min	0.94	0.99	0.22	− 0.26	6.02	[− 12.06, 11.55]
70 min	0.94	0.99	0.22	− 0.24	6.04	[− 12.08, 11.60]
60 min	0.94	0.99	0.22	− 0.16	6.08	[− 12.07, 11.75]
50 min	0.94	0.99	0.23	− 0.10	6.07	[− 12.01, 11.80]
MRTM2 R_1						
90 min	0.94	0.99	0.21	− 0.37	5.83	[− 11.79, 11.05]
80 min	0.94	0.99	0.22	− 0.32	5.89	[− 11.87, 11.23]
70 min	0.94	0.99	0.22	− 0.29	5.93	[− 11.91, 11.33]
60 min	0.94	0.99	0.23	− 0.21	6.11	[− 12.18, 11.75]
50 min	0.94	0.99	0.22	0.06	6.07	[− 11.83, 11.95]

reference tissue model. Since this approach takes into account relative changes in tracer delivery [20], a reference tissue model using a 60-min dynamic PET scan would be preferred for monitoring longitudinal changes. Moreover, the corresponding R_1 maps could have an added value for the differential diagnosis between different disease types [21–24], On the other hand, the clinical applicability of this approach is limited because of the 1-h acquisition time. Therefore, we also considered a static SUVR approach relative to SO using a shorter static [^{11}C]UCB-J PET scan, since this approach could be preferred for studying synaptic pathology in specific patients groups such as cognitive impaired patients or patients with stroke and movement disorders. For this study, we used a 30-min acquisition time starting at 60 min, 50 min, and 40 min respectively, after tracer injection. Although a shorter static frame time could be considered, a 30-min acquisition time interval was selected to allow the simultaneous acquisition of structural and functional MRI data, including perfusion MRI data using arterial spin labeling (ASL). This way, one can take full advantage of simultaneous PET/MR imaging by combining MR perfusion maps with static [^{11}C]UCB-J

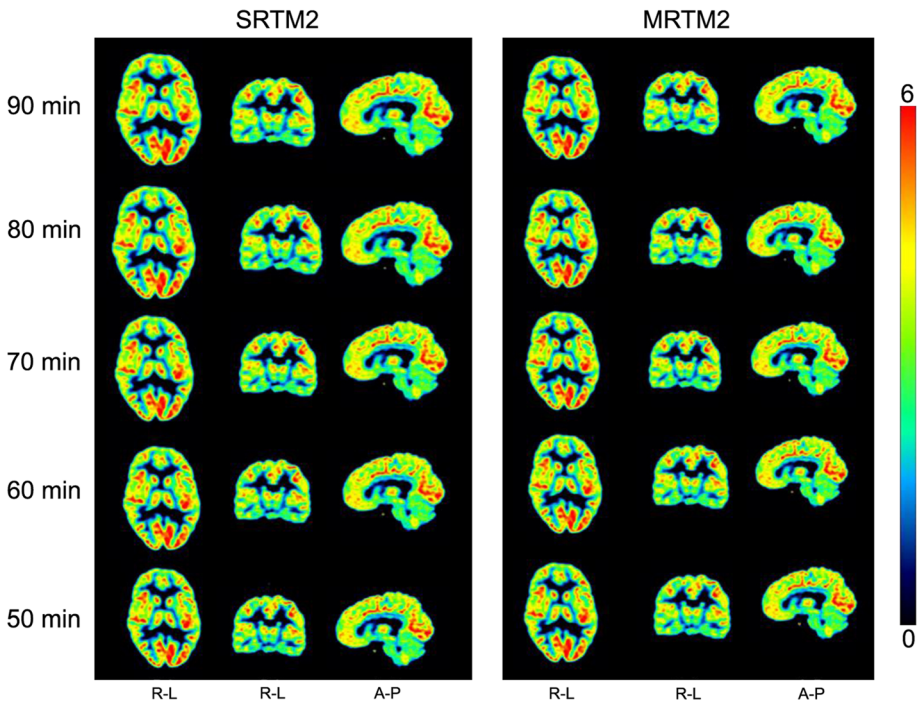

Fig. 4 Parametric R_1 maps of a baseline scan of a healthy volunteer (M, 23 years, 93 kg, 197 MBq [^{11}C]UCB-J) using the centrum semi-ovale (SO) as reference tissue.

PET scan as an alternative for the relative perfusion maps or R_1 maps generated by reference tissue approaches using longer, dynamic [^{11}C]UCB-J PET scanning protocols.

We did not limit our study to baseline [^{11}C]UCB-J PET imaging of the human brain but also considered dynamic [^{11}C]UCB-J PET data after administration of a novel drug with high affinity for presynaptic SV2A. The reduced [^{11}C]UCB-J PET signal, because of the blocking effect of the drug, could be considered as representative for pathologically reduced synaptic density. Linear regression and correlation results for both baseline and post drug scans were reported separately, as well as combined, to validate parametric reference tissue approaches for both conditions. Since post drug [^{11}C]UCB-J kinetics of the scans were faster, a reduction of the acquisition time was expected to be less critical for post drug PET scanning. This was confirmed by the linear regression analysis showing that the goodness of fit to a straight line is improved for post drug [^{11}C]UCB-J scanning compared to baseline [^{11}C]UCB-J scanning especially for shorter acquisition times (see Table 1).

For pooled baseline and post dose scans, rLGA using a 90-min dynamic [^{11}C]UCB-J PET scan and $SUVR_{SO,40–70}$ demonstrated a lower performance compared to the other parametric reference tissue approaches. These findings were also confirmed by the Bland-Altman analysis comparing each of the parametric approaches with regional 1TCM DVR_{SO} values. Again, baseline findings were reported separately using a percentage differences plot, while overall findings were reported using a unit differences plot because of the small 1TCM DVR_{SO} values around 1 for post drug scanning under nearly full blocking conditions.

The lower performance of rLGA for a 90-min dynamic [^{11}C]UCB-J PET scan is in line with the previously reported, noise-induced negative biases of rLGA-based DVR estimates [25]. Although graphical methods such as rLGA do not make assumptions about the compartmental configuration of the underlying data and are easier to perform because they are less computer intensive, the noise in the PET TACs is propagated as correlated errors in dependent and independent variables of the rLGA equation, resulting in increasing underestimation of DVR with increasing noise. On the other hand, MRTM2 partially mitigate this issue for rLGA, by using less noisy tissue data in the independent variables while a basis function implementation of SRTM2 is computationally efficient [17]. Moreover, the 1TCM model requirements for SRTM2 and MRTM2 are fulfilled for [^{11}C]UCB-J tracer kinetics in target and reference tissue and both parametric methods also provide R_1 maps relative to SO next to the BP_{SO} maps. Therefore, we did not consider the rLGA approach for a time stability analysis and limited this analysis to MRTM2 and SRTM2. Results indicated that both SRTM2 and MRTM2 provided accurate parametric $BP_{SO}+1$ maps for an acquisition time of at least 60 min (−1.0 % bias +9.9 % variability for SRTM2); while for a shorter acquisition time of 50 min, bias increased to −6.5 % with 11.4 % variability, which is in line with literature data [12, 26]. Time stability results from the non-linear method SRTM2 performed better than estimates from the graphical approach MRTM2 suffer from increased statistical noise. In terms of parametric R_1 maps, indicative for relative blood flow, a reduction of the acquisition time down to 50 min did not impact the regional quantitative accuracy of both SRTM2 and MRTM2 R_1 maps (see Table 3).

For a static SUVR approach, $SUVR_{SO,50–80}$ and $SUVR_{SO,60–90}$ proved to be valid quantitative proxies for parametric BP_{so} map. Regional $SUVR_{SO,40–70}$ values showed a negative bias of 7.8 %, which was significantly less accurate than the SUVR data for later acquisition time intervals. This is probably because pseudo-equilibrium has not been reached yet for the 40- to 70-min acquisition time interval.

Considering the limitations of this study, no test-retest variability data were available for the dynamic parametric approaches and SUVR-based quantification approaches. A mean absolute test-retest reproducibility of 3–9 % across brain regions was reported for [^{11}C]UCB-J V_T values by other authors [26, 27]. Since a non-invasive reference tissue approach alleviates the need for a cross-calibration of PET scanner and dose calibrator and avoids the logistically challenging arterial blood sampling, a full image–based quantification approach will generally not increase test-retest variability. However, limited count statistics in the reference region due to the lower tracer uptake or restricted size can have a negative impact on test-retest variability of BP_{SO} and SUVR estimates. These challenges were previously described in literature by Koole et al. [13]. Moreover, it has been demonstrated for amyloid PET imaging that blood flow changes introduced alterations in cortical SUVR relative to either white matter or cerebellum and that SUVR relative to white matter was more affected by global blood flow changes [28–30]. Therefore, a simulation study could be considered to evaluate the effect of blood flow changes in SO and cortical target regions on a SUVR quantification relative to SO. Furthermore, it would also be worthwhile to reevaluate parametric reference tissue methods for [^{11}C]UCB-J PET imaging in patient groups, especially if pathological white matter involvement is expected (*e.g.*, in neuro-inflammatory disorders and several neurodegenerative diseases [31]) and SO as reference region needs to be restricted to voxels with confirmed white matter integrity. Quantification linked to these white matter lesions should be evaluated as a pseudo-reference region approach, including a robust partial volume correction for smaller reference regions in patient groups to ensure sufficient count statistics.

Conclusion

Both SRTM2 and MRTM2 provided more robust [^{11}C]UCB-J parametric maps compared to rLGA; while for shorter acquisition times, SRTM2 BP_{ND} proved to be more in agreement with 1TCM DVR compared to MRTM2. Therefore, SRTM2 is the preferred parametric method for voxelwise analysis of dynamic [^{11}C]UCB-J PET studies using SO as reference tissue. In order to obtain quantitatively accurate parametric BP_{SO} and R_1 maps, a dynamic PET scan of at least 60 min is required. To improve clinical

applicability, $SUVR_{SO}$ images relative to SO using a 30-min static [^{11}C]UCB-J PET scan starting at either 50 or 60 min after tracer injection can be considered as an excellent proxy for parametric BP_{SO} maps.

Acknowledgments. The authors thank the participants in addition to the investigators and their teams who contributed to this study. We also thank Kwinten Porters and Jef Van Loock (department Nuclear Medicine, UZ Leuven) for their technical assistance, and the UZ Leuven radiopharmacy team for the tracer productions. We also acknowledge Barbara Pelgrims, PhD, (UCB Pharma, Brussels, BE) for publication coordination.

Funding Information. Part of this study was sponsored by a UCB Pharma research grant of UCB-J to KU Leuven (principal investigator Koen Van Laere).

Compliance with Ethical Standards

Conflict of Interest

Ralph Paul Maguire, Brigitte Lacroix, Joel Mercier, and David Sciberras are employees of UCB Pharma. Nathalie Mertens, Kim Serdons, Koen Van Laere, and Michel Koole have no conflicts of interest to disclose.

Ethical Approval

All procedures performed in studies involving human participants were in accordance with the ethical standards of the institutional and/or national research committee and with the 1964 Helsinki declaration and its later amendments or comparable ethical standards. All subjects signed informed consent before entering the study.

References

1. Crevecoeur J, Kaminski RM, Rogister B et al (2014) Expression pattern of synaptic vesicle protein 2 (SV2) isoforms in patients with temporal lobe epilepsy and hippocampal sclerosis. Neuropathol Appl Neurobiol 40:191–204
2. Feng G, Xiao F, Lu Y, Huang Z, Yuan J, Xiao Z, Xi Z, Wang X (2009) Down-regulation synaptic vesicle protein 2A in the anterior temporal neocortex of patients with intractable epilepsy. J Mol Neurosci 39:354–359
3. Proper EA, Oestreicher AB, Jansen GH, Veelen CWM, van Rijen PC, Gispen WH, de Graan PNE (2000) Immunohistochemical characterization of mossy fibre sprouting in the hippocampus of patients with pharmaco-resistant temporal lobe epilepsy. Brain 123:19–30
4. DeKosky ST, Scheff SW (1990) Synapse loss in frontal cortex biopsies in Alzheimer's disease: correlation with cognitive severity. Ann Neurol 27:457–464
5. Hamos JE, DeGennaro LJ, Drachman DA (1989) Synaptic loss in Alzheimer's disease and other dementias. Neurology 39:355–361
6. Tang G, Gudsnuk K, Kuo SH, Cotrina ML, Rosoklija G, Sosunov A, Sonders MS, Kanter E, Castagna C, Yamamoto A, Yue Z, Arancio O, Peterson BS, Champagne F, Dwork AJ, Goldman J, Sulzer D (2014) Loss of mTOR-dependent macroautophagy causes autistic-like synaptic pruning deficits. Neuron 83:1131–1143
7. Kang H, Voleti B, Hajszan T et al (2012) Decreased expression of synapse-related genes and loss of synapses in major depressive disorder. Nat Med 18:1413–1417
8. Glantz LA, Lewis DA (2000) Decreased dendritic spine density on prefrontal cortical pyramidal neurons in schizophrenia. APN 57:65–73
9. Sekar A, Bialas AR, de Rivera H et al (2016) Schizophrenia risk from complex variation of complement component 4. Nature 530:177–183
10. Bajjalieh SM, Frantz GD, Weimann JM, McConnell S, Scheller RH (1994) Differential expression of synaptic vesicle protein 2 (SV2) isoforms. J Neurosci 14:5223–5235
11. Finnema SJ, Nabulsi NB, Eid T et al (2016) Imaging synaptic density in the living human brain. Sci Transl Med 8:348–396
12. Nabulsi NB, Mercier J, Holden D, Carre S, Najafzadeh S, Vandergeten MC, Lin SF, Deo A, Price N, Wood M, Lara-Jaime T, Montel F, Laruelle M, Carson RE, Hannestad J, Huang Y (2016) Synthesis and preclinical evaluation of ^{11}C-UCB-J as a PET tracer for imaging the synaptic vesicle glycoprotein 2A in the brain. J Nucl Med 57:777–784
13. Koole M, van Aalst J, Devrome M et al (2018) Quantifying SV2A density and drug occupancy in the human brain using [^{11}C]UCB-J PET imaging and subcortical white matter as reference tissue. Eur J Nucl Med 1619–7089
14. Hammers A, Allom R, Koepp MJ, Free SL, Myers R, Lemieux L, Mitchell TN, Brooks DJ, Duncan JS (2003) Three-dimensional maximum probability atlas of the human brain, with particular reference to the temporal lobe. Hum Brain Mapp 19:224–247
15. Cunningham VJ, Rabiner EA, Slifstein M, Laruelle M, Gunn RN (2010) Measuring drug occupancy in the absence of a reference region: the Lassen plot re-visited. J Cereb Blood Flow Metab 30:46–50
16. Gunn R, Lammertsma A, Hume S et al (1997) Parametric imaging of ligand-receptor binding in PET using a simplified reference region model. Neuroimage 6(4):279–287
17. Ichise M, Liow JS, Lu JQ, Takano A, Model K, Toyama H, Suhara T, Suzuki K, Innis RB, Carson RE (2003) Linearized reference tissue parametric imaging methods: application to [^{11}C]DASB positron emission tomography studies of the serotonin transporter in human brain. J Cereb Blood Flow Metab 23:1096–1112
18. Logan J, Fowler JS, Volkow ND, Wang GJ, Ding YS, Alexoff DL (1996) Distribution volume ratios without blood sampling from graphical analysis of PET data. J Cereb Blood Flow Metab 16:834–840
19. Wu Y, Carson RE (2002) Noise reduction in the simplified reference tissue model for neuroreceptor functional imaging. J Cereb Blood Flow Metab 22:1440–1452
20. Lammertsma (2017) Forward to the past: the case for quantitative PET imaging. J Nucl Med 58:1019–1024
21. Meyer PT, Hellwig S, Amtage F, Rottenburger C, Sahm U, Reuland P, Weber WA, Hull M (2011) Dual-biomarker imaging of regional cerebral amyloid load and neuronal activity in dementia with PET and ^{11}C-labeled Pittsburgh compound B. J Nucl Med 52:393–400
22. Appel L, Jonasson M, Danfors T, Nyholm D, Askmark H, Lubberink M, Sorensen J (2015) Use of ^{11}C-PE2I PET in differential diagnosis of parkinson disorders. J Nucl Med 56:234–242
23. Jonasson M, Appel L, Dansfors T et al (2017) Development of a clinically feasible [^{11}C]PE2I PET method for differential diagnosis of parkinsonism using reduced scan duration and automated reference region extraction. Am J Nucl Med Mol Imaging 7:263–274
24. Peretti DE, Vallez Garcia D, Reesink FE et al (2019) Relative cerebral flow from dynamic PIB scans as an alternative for FDG scans in Alzheimer's disease PET studies. PLoS One 14:e0211000
25. Slifstein M, Laruelle M (2000) Effects of statistical noise on graphic analysis of PET neuroreceptor studies. J Nucl Med 41:2083–2088
26. Finnema SJ, Nabulsi NB, Mercier J et al (2017) Kinetic evaluation and test-retest reproducibility of [^{11}C]UCB-J, a novel radioligand for positron emission tomography imaging of synaptic vesicle glycoprotein 2A in humans. J Cereb Blood Flow Metab 38:2041–2052
27. Van Laere K, Ahmad RU, Hudyana H et al (2013) Quantification of ^{18}F-JNJ-42259152, a novel phosphodiesterase 10A PET tracer: kinetic modeling and test-retest study in human brain. J Nucl Med 54:1285–1293
28. Ottoy J, Verhaeghe J, Niemantsverdriet E, Engelborghs S, Stroobants S, Staelens S (2017) A simulation study on the impact of the blood flow-dependent component in [^{18}F]AV45 SUVR in Alzheimer's disease. PLoS One 12:e0189155
29. Cselényi Z, Farde L (2015) Quantification of blood flow-dependent component in estimates of beta-amyloid load obtained using quasi-steady-state standardized uptake value ratio. J Cereb Blood Flow Metab 35:1485–1493
30. van Berckel BN, Ossenkoppele R, Tolboom N et al (2013) Longitudinal amyloid imaging using ^{11}C-PiB: methodologic considerations. J Nucl Med 54:1570–1576
31. Barber R, Scheltens P, Gholkar A, Ballard C, McKeith I, Ince P, Perry R, O'Brien J (1999) White matter lesions on magnetic resonance imaging in dementia with Lewy bodies, Alzheimer's disease, vascular dementia, and normal aging. J Neurol Neurosurg Psychiatry 67:66–67